ISSN: 2688-8645

Research on Torque Characteristics of Magnetic Transmission Mechanism of Electric Submersible Centrifugal Pump

Haowei Qin, Jun Shao, Jiawei Wang, Qi Zhang

College of Mechanical Engineering, Xi'an Shiyou University, Xi'an Shaanxi, 710065, China

Abstract

This study presents a non-contact magnetic drive scheme designed to eliminate leakage at dynamic seals in Electric Submersible Centrifugal Pumps (ESPs) operating in high-temperature downhole environments (up to 200°C). The torque performance, magnetic field distribution, and eddy current losses of the proposed cylindrical magnetic coupling were investigated through integrated theoretical analysis and finite element (FE) simulations. A magnetic torque formula was derived theoretically, leading to the selection of Samarium-Cobalt (SmCo) permanent magnets and the determination of their axial length required for a 149.2 N·m torque output. FE simulations conducted in ANSYS Maxwell predicted a maximum static flux density of 2.397 T and a transient magnetic torque of 165 N·m, which deviates from the theoretical value by about 10.59%. The eddy current loss in the isolation sleeve was assessed to be 348.95 W. Three-dimensional simulations further highlighted the impact of end effects, prompting an optimization recommendation to use soft magnetic end caps for reduced flux leakage. The findings confirm the feasibility of the magnetic drive mechanism as an effective seal for ESPs, offering valuable design insights for magnetic transmission systems under extreme temperature and pressure.

Keywords

Electric Submersible Centrifugal Pump; Magnetic Drive; Magnetic Transmission; Torque Calculation; Finite Element Analysis.

1. Introduction

Magnetic drive technology, with its characteristics of non-contact power transmission and magnetic field coupling for sealing, has become a key technology for solving dynamic seal leakage problems in rotating machinery. It is widely used in devices such as magnetic drive pumps [1], couplings[2], magnetic drive mud pumps [3], and downhole motors [4]-[5]. However, the transmission performance of this technology, particularly its core output metric—magnetic torque—is highly dependent on the rational design and precise calculation of the magnetic circuit structure [6]-[8]. Methods for calculating magnetic torque are numerous and complex, with the magnetostatic energy method [9]and the analytical method based on Gauss's theorem for magnetic fields being important theoretical foundations commonly used in engineering. Meanwhile, parameters such as magnet pole configuration and permanent magnet material significantly affect torque and efficiency. To address the leakage problem in Electric Submersible Centrifugal Pumps (ESPs), this paper focuses on the magnetic circuit design of their magnetic drive mechanism. The research integrates theoretical calculation and finite element simulation, with a focus on analyzing the magnetic field distribution, torque transmission characteristics, and eddy current losses. This work aims to provide a theoretical basis for the design of high-performance transmission solutions applied in high-temperature downhole environments (200°C).

ISSN: 2688-8645

2. Theoretical and Computational Basis

2.1. Fundamental Principles and Structure

The basic structure of the Electric Submersible Centrifugal Pump (ESP) based on the magnetic drive mechanism is shown in Figure 1. Its core operating principle lies in utilizing the magnetic field coupling of permanent magnets to achieve non-contact power transmission. Specifically, the output torque of the submersible motor drives the outer magnetic rotor to rotate via a drive shaft. Through the interaction of their permanent magnetic fields, the outer and inner magnetic rotors transmit torque across the isolation can to the pump shaft connected to the inner rotor, ultimately driving the centrifugal pump impeller. In this configuration, the isolation can provides a complete static seal between the submersible motor and the pump, thereby fundamentally preventing the wear and leakage issues associated with traditional mechanical shaft seals.

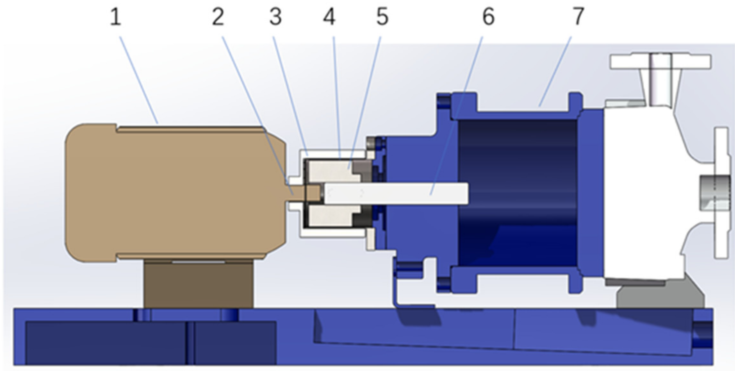

1. Submersible Motor;2. Motor Shaft;3. Outer Magnetic Rotor;4. Isolation Can;
5. Inner Magnetic Rotor;6. Pump Shaft;7. Submersible Centrifugal Pump;

Figure 1. Schematic diagram of the magnetically driven electric submersible centrifugal pump.

The isolation can is a complete thin-walled cylinder. One end is securely connected to the pump body, while the other end is sealed to the motor housing or an intermediate housing. This configuration physically separates the pump chamber, which is filled with the working medium, from the clean and dry motor chamber. The task of power transmission is undertaken by the inner and outer magnetic rotors, positioned on the inner and outer sides of the isolation can, respectively. These rotors establish a robust coupling magnetic field through the use of high-performance permanent magnet materials. When the motor drives the outer rotor to rotate, the changing magnetic field penetrates the static barrier of the isolation can without contact, compelling the inner rotor—immersed in the medium—to rotate synchronously. This, in turn, drives the pump impeller to perform work. Consequently, the dynamic sealing interface that rotates with the shaft in traditional designs is eliminated. The power transmission path and the medium flow path are spatially separated. All sealing requirements are simplified and consolidated at the static connections between the isolation can and the fixed housings, achieved via gaskets or O-rings. The reliability of such static seals is readily achievable and assured in engineering practice.

2.2. Cylindrical Magnetic Drive Mechanism

The cylindrical magnetic drive mechanism consists of coaxially arranged inner and outer cylindrical magnetic rotors. As shown in Figure 2, in the concentric state, the N-pole (S-pole) of the inner rotor and the S-pole (N-pole) of the outer rotor are axially aligned due to magnetic attraction. In this state, there is no tangential electromagnetic force component between the

ISSN: 2688-8645

two rotors, resulting in zero output torque. When a driving torque is applied to either rotor, it initiates rotational motion. At the initial stage of motion, the other rotor remains stationary due to static friction and load resistance, causing a relative angular displacement between the inner and outer magnetic poles. This displacement disrupts the initial alignment of the poles: the N-pole (S-pole) of the outer rotor exerts a magnetic attractive force on the adjacent S-pole (N-pole) of the inner rotor, generating a tangential pulling force. Simultaneously, the same outer rotor pole experiences a tangential pushing force from the magnetic repulsion with the adjacent inner rotor pole of the same polarity (N-pole or S-pole). This combined push-pull force creates a net torque that drives the two rotors to rotate synchronously. When the centerline of an inner rotor pole is positioned midway between two opposite-polarity poles of the outer rotor, this tangential push/pull force reaches its peak, thereby achieving maximum power transmission efficiency.

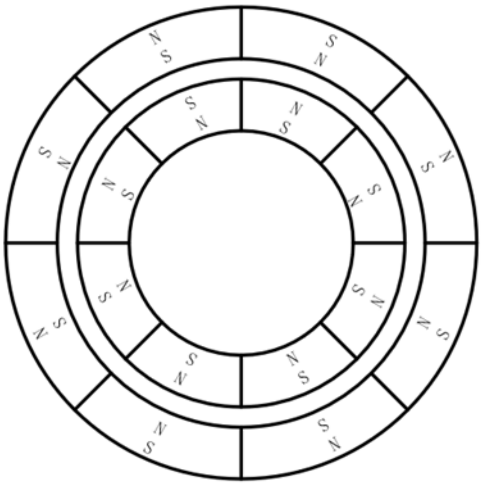

Figure 2. Magnetic Field Model of the Cylindrical Magnetic Drive Mechanism

The core components of the cylindrical magnetic drive mechanism include the yoke, permanent magnets, encapsulation layer, and the isolation can. In the application for electric submersible centrifugal pumps, the output shaft of the submersible motor is connected to the mechanism's outer magnetic rotor, while the inner magnetic rotor is coupled to the submersible pump shaft. The magnetic field force coupling generated by the outer rotor drives the rotation of the inner rotor, thereby transmitting the mechanical energy from the submersible motor to the pump shaft without contact. Since the power transmission is accomplished entirely through the magnetic field, no mechanical linkage components are required on either side of the isolation can. Consequently, this mechanism constitutes a fully static-seal power transmission system, ensuring zero leakage of the medium.

Furthermore, due to the non-contact transmission characteristic between the inner and outer rotors, there is no rigid connection between them. Therefore, if the outer rotor experiences sudden speed changes or vibrations, the energy is not directly transferred to the inner rotor. Conversely, dynamic disturbances of the inner rotor likewise do not affect the operational state of the outer rotor. This inherent vibration isolation mechanism enables the cylindrical magnetic drive mechanism to effectively ensure the stable operation of the electric submersible centrifugal pump.

2.3. Theoretical Calculations

In current engineering practice, the magnetic torque is commonly calculated using Gauss's theorem. The simplified formula for its maximum value is given below[10]:

$$T = \left(\frac{1}{5000}\right)^2 KMHmSt_h R_c \sin\left(\frac{m}{2}\phi\right) \quad (1)$$

In the formula:

T – Magnetic torque, N·m.

K – Magnetic circuit coefficient. The value of K exhibits significant configuration dependence. In combined push-pull magnetic circuit designs, its typical range is 4.0 to 6.4.

M – Magnetization intensity, $M = (B_m + H_m)/4\pi$, where B_m and H_m are the magnetic flux density and magnetic field strength at the operating point, respectively. Unit:Gs.

H – Magnetic field strength generated by the outer magnetic circuit at the inner rotor, Oe. $H = N_1 \times 4\pi m\left(1 - \frac{t_g}{\sqrt{t_g^2 + t_0^2}}\right)\eta$ Where: N_1 is the empirical coefficient for magnet pole shape (1.24 for rectangular poles, 1.05 for sector-shaped poles);

t_g is the working air-gap thickness, cm;

η is the pole thickness coefficient ($\eta \approx 0.95$ when $t_0/t_h = 0.7$–0.9).

m – Number of magnetic pole pairs.

S – Pole area, $S = t_0 L$, cm^2.

t_h – Average pole thickness, cm.

R_c – Average rotational radius of the magnetic rotor, $R_c = (R_2 + R_3)/2$, cm.

φ – Magnetic axis offset angle during operation, degrees.

Based on Equation (1) and the selection of corresponding coefficients, where the magnetic circuit coefficient K is set to 6.4, the magnetization intensity is taken as 7000 Gs, and both the inner and outer magnetic segments adopt a sector-shaped structure (resulting in an empirical shape coefficient of 1.04), the magnetic field strength H generated by the outer magnetic circuit at the location of the inner magnet is determined. Through analytical derivation, the expression for the axial length of the permanent magnet is obtained as follows:

$$L = \frac{2.49 \times 10^6 T_{\max}}{MH(R_2 + R_3)^2 t_h} \tag{2}$$

As the core power unit of the electric submersible pump system, the submersible motor typically adopts a slender-designed squirrel-cage three-phase induction motor. For this design, the submersible motor model YQY143-45s-FF/GZ is selected as the research subject. This motor has a power rating of 45 kW and a rated speed of 2880 r/min, thus requiring a maximum torque of 149.2 N·m. Based on these requirements, the calculated necessary parameters are listed in Table 1.

Table 1. Design Input Parameters for Permanent Magnet Length Calculation in the Magnetic Drive Mechanism

Parameter	Value	Parameter	Value
Permanent Magnet Material	Samarium Cobalt (SmCo)	Magnetization Intensity M (T)	0.7
Empirical Coefficient N_1	1.04	Magnetic Circuit Coefficient K	6.4
Working Air Gap Thickness t_g (mm)	1.5	Average Pole Thickness t_h(cm)	25
Inner Rotor Inner Radius R_1 (mm)	12.5	Inner Rotor Outer Radius R_2(mm)	37.5
Outer Rotor Inner Radius R_3 (mm)	39	Outer Rotor Outer Radius R_4 (mm)	64
Number of Pole Pairs m	8	Pole Thickness Coefficient η	0.95

ISSN: 2688-8645

Combining the required axial length L of the SmCo permanent magnet from Equation (2) mentioned above, the theoretical calculation result is 41.32 cm. Considering the influence of factors such as friction and magnetic flux leakage, the value is taken as L = 43 cm for the design. Substituting this value into the magnetic torque formula for verification yields a theoretical torque of 154.72 N·m, which meets the design requirements.

2.4. Arrangement

In the design of magnetic drive systems, the magnet configuration scheme directly affects torque transmission characteristics. Early designs commonly employed single-row spaced magnetic circuit layouts. With advancements in permanent magnet material technology, new configurations such as single-row compact, single-row flux-focusing, and multi-row flux-focusing types have gradually emerged. In current engineering practice, the combined push-pull magnetic circuit has become the mainstream solution due to its outstanding transmission efficiency; therefore, this optimized configuration is adopted in this paper.

The number of magnetic poles, as another critical parameter, has an optimal range—both too many and too few poles lead to torque attenuation. Engineering experience indicates that, except for special conditions such as high power, high rotational speed, or wide air gaps, the optimal pole count typically falls within the even-numbered range of 8 to 30. This study initially sets 8 sets of radially magnetized permanent magnets, arranged alternately as N and S poles to form the fundamental magnetic circuit[11]. This parameter will subsequently be refined and validated through electromagnetic field simulation.

2.5. Material Selection

In the magnetic drive mechanism, permanent magnets serve as the core components for generating the coupled magnetic field. Their magnetic properties directly determine the transmission torque, operational efficiency, and reliability of the mechanism. Given the application requirements of the downhole high-temperature environment (200°C), the material's temperature resistance and thermal stability become critical selection criteria. It is essential that the material maintains stable magnetic properties and avoids irreversible demagnetization within the operating temperature range, characterized by a low reversible temperature coefficient of remanence and a high Curie temperature.

Currently, high-performance permanent magnet materials commonly used in engineering mainly include ferrites, samarium-cobalt (SmCo), and neodymium-iron-boron (NdFeB). Considering the specific application scenario of this design—the harsh high-temperature constraints faced by downhole oil drilling and production equipment—along with the material performance requirements, particularly high-temperature stability and resistance to demagnetization, SmCo permanent magnets have been selected as the most suitable choice due to their outstanding high-temperature performance.

Within the magnetic drive mechanism, the permanent magnets are fixed to the inner and outer rotor cores (yokes). The magnetic flux generated by the magnets must form a complete closed loop through these core materials. Therefore, the core material must be a soft magnetic material with excellent magnetic permeability. Such materials serve two primary functions: firstly, to shield against external magnetic interference through the magnetic shielding effect, ensuring operational stability; and secondly, to optimize flux leakage by regulating the magnetic flux distribution.

The selection of soft magnetic materials focuses on three core parameters: high permeability to ensure efficient magnetic circuit conduction, low coercivity to reduce hysteresis losses, and high saturation magnetization to enhance magnetic load capacity. Common industrial choices include industrial pure iron, silicon steel, and iron-nickel alloys. As the mechanism operates under a static magnetic field, alternating magnetic losses need not be considered. Consequently, while meeting the magnetic performance requirements, priority is given to the material's manufacturability and cost-effectiveness. Silicon steel is ultimately selected as the core material. Its permeability is significantly higher than that of low-carbon steel, and it offers lower cost and ease of machining. This material not only efficiently closes the magnetic circuit but its relatively high resistivity also helps suppress eddy currents, making it well-suited for use in static magnetic fields.

The isolation can, serving as the core sealing and pressure-bearing component of the magnetic drive system, is installed within the dynamic working air gap between the inner and outer magnetic rotors. Its primary function is to achieve fully sealed operation of the drive chamber, isolating it from the erosive external drilling fluid. This component operates under extreme conditions, simultaneously facing three major challenges: comprehensive stress from medium abrasion and the downhole high-temperature, high-pressure environment; eddy current losses induced by the changing magnetic field; and periodic pressure loads generated by the rotating fluid. Therefore, the isolation can material must comprehensively satisfy the requirements of high resistivity (to suppress eddy currents), high strength and corrosion resistance (to ensure reliable pressure-bearing with a thin wall), and good manufacturability.

Through comprehensive comparison and selection, titanium alloy TC4 is chosen for the isolation can in this study. Its high resistivity (approximately 1.62 μΩ·m) effectively controls eddy current heating. Its high tensile strength (895 MPa) meets the requirements for thin-wall pressure bearing and impact resistance. Furthermore, it possesses excellent corrosion resistance. Thus, titanium alloy TC4 enables the simultaneous achievement of the core objectives in extreme operating conditions: reliable sealing, high magnetic circuit efficiency, and long-term stable operation.

3. Magnetic Field Simulation and Analysis

Based on the aforementioned parameters, simplified two-dimensional (2D) and three-dimensional (3D) models of the magnetic drive mechanism were established in ANSYS Maxwell, as illustrated in Figure 3. The model consists, from the inner to the outer region, of the inner yoke, inner permanent magnets, isolation can, outer permanent magnets, and outer yoke. The yoke material is silicon steel, the isolation can is titanium alloy, the permanent magnets are samarium-cobalt (SmCo), and the remaining domains are assigned as air. An infinite boundary condition was applied to the outermost air region, while natural boundary conditions were automatically applied by the software to the inner surface of the inner yoke and the outer surface of the outer yoke. The models were meshed using tetrahedral elements. Static and transient magnetic field simulations were performed on the 2D model, whereas only static magnetic field analysis was conducted for the 3D model.

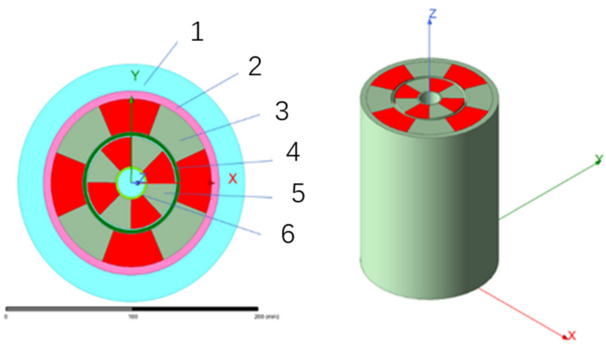

1. Air (Solution Domain);2. Outer yoke;3. Outer magnetic rotor;4. Isolation can;
5. Inner magnetic rotor6. Inner yoke

Figure 3. Finite element simulation model of the magnetic drive mechanism.

3.1. Static Magnetic Field Analysis of the 2D Model

When the magnetic drive mechanism is stationary, the overall magnetic flux density distribution of the model is shown in Figure 4. The inner and outer yokes are made of silicon steel, which possesses high magnetic permeability, allowing the magnetic field to easily pass through and form a closed loop. The maximum magnetic flux density occurs at the yoke regions where the two permanent magnets interface, reaching a peak value of 2.397 T.

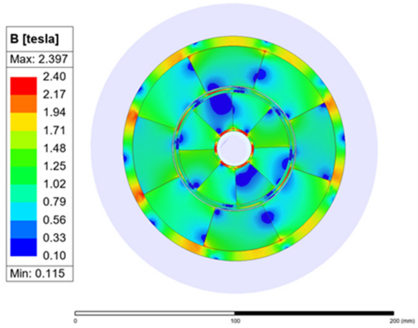

Figure 4. Magnetic flux density distribution in the 3D model of the magnetic drive mechanism.

The distribution curve of magnetic flux density along the circumferential direction at the outer diameter of the inner magnetic rotor is shown in Figure 5. It can be observed that the magnetic flux density exhibits a periodic distribution along the circumference, and the number of periods corresponds to the number of permanent magnets. This indicates that the overall magnetic field within the magnetic drive mechanism is formed by the superposition of the magnetic fields generated by all individual permanent magnets.

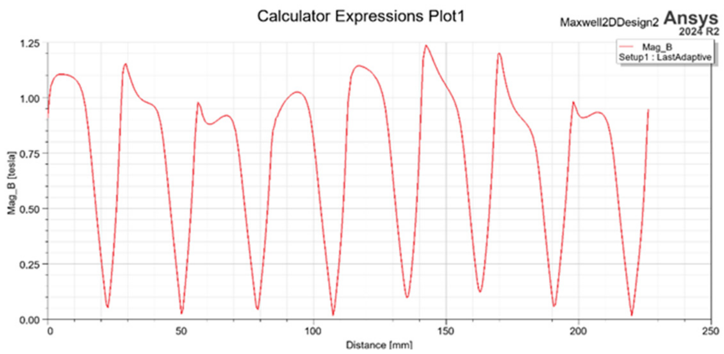

Figure 5. Circumferential magnetic flux density distribution at the inner rotor outer diameter.

3.2. Transient Magnetic Field Analysis of the 2D Model

In actual operation, the isolation can remains stationary while the inner and outer magnetic rotors rotate synchronously. For the transient magnetic field simulation, the inner and outer rotors were held stationary. Instead, a band region was assigned to the isolation can, imposing a rotational motion of 2800 r/min. Due to the principle of electromagnetic induction (Faraday's law), this motion induces eddy currents within the isolation can. The resulting ohmic loss density distribution on the isolation can is presented in Figure 6.

As shown in Figure 7, the maximum ohmic loss density, reaching 7.453×10^{6} W/m^3, occurs at locations where the magnetic poles of the inner and outer permanent magnets are opposite (i.e., where the magnetic flux lines penetrate). This is precisely where the magnetic field interaction and induced eddy currents are strongest.

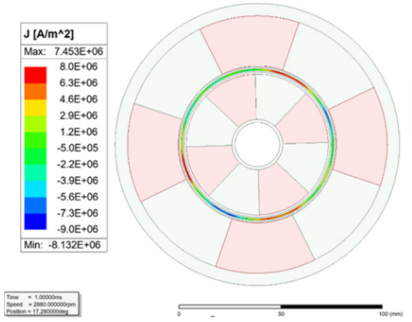

Figure 6. Distribution of ohmic loss density in the isolation can.

The eddy current loss density within the isolation can region was integrated over its volume via the field calculator, yielding a calculated loss value of 811.05 W. Since the 2D magnetic field simulation in ANSYS Maxwell assumes a default axial length (Z-direction) of 1 m, this result was scaled according to the actual axial dimension of 0.43 m. Consequently, the actual eddy current loss for the isolation can was determined to be 348.95 W.

From the calculation results, the simulated maximum magnetic torque was obtained as 165 N·m. This value meets the design requirements. Compared with the theoretical value, the relative error is approximately 10.59%. The sources of this error are analyzed as follows: (1) The magnetic torque calculation formula based on Gauss's theorem requires the selection of an empirical coefficient, and the formula itself carries an inherent error of around 10%; (2) Errors are introduced by the mesh generation and solution methods within the ANSYS Maxwell software.

3.3. Static Magnetic Field Analysis of the 3D Model

The two-dimensional (2D) model neglects the influence of end effects and the axial distribution of the magnetic field on the magnetic drive mechanism. Therefore, a three-dimensional (3D) analysis is necessary. The magnetic flux density distribution of the 3D model is shown in Figure 7. It can be observed from Figure 7 that the maximum magnetic flux density is 2.179 T. Compared to the maximum value from the 2D model, this represents a reduction of 9.09%. This discrepancy is attributed to the axial magnetic flux leakage at the ends of the inner and outer magnetic rotors, which was not accounted for in the 2D analysis.

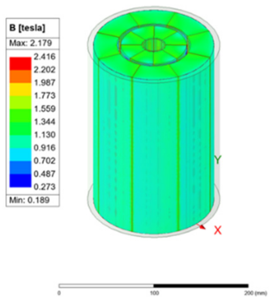

Figure 7. Distribution of magnetic flux density in the 3D model of the magnetic drive mechanism.

4. Conclusion

If you follow the "checklist" your paper will conform to the requirements of the publisher and facilitate a problem-free publication process.

To address the leakage issue in Electric Submersible Centrifugal Pumps (ESPs) under high-temperature downhole conditions (200°C), this paper proposes a non-contact sealing transmission scheme based on a magnetic drive mechanism. A combined approach of theoretical calculation and finite element analysis (FEA) was employed to systematically investigate the torque characteristics, magnetic field distribution, and eddy current losses of the mechanism, providing theoretical foundations and engineering references for magnetic drive design in high-temperature and high-pressure applications.

The study first derived a theoretical formula for calculating magnetic torque based on Gauss's theorem, determining the magnetic circuit parameters with Samarium-Cobalt (SmCo) permanent magnets as the core. The required axial length of the permanent magnets to meet the torque demand of 149.2 N·m was calculated. Subsequently, two-dimensional (2D) and three-dimensional (3D) finite element models of the magnetic drive mechanism were established using ANSYS Maxwell software for static and transient magnetic field simulations. The results indicate that the designed mechanism exhibits a reasonable static magnetic flux density distribution with a maximum value of 2.397 T. In the transient analysis, the eddy current loss in the isolation can was 348.95 W, and the simulated magnetic torque was 165 N·m, showing an error of approximately 10.59% compared to the theoretical value, which meets the design requirements. Furthermore, the 3D simulation revealed the influence of end effects on the magnetic field distribution.

This research verifies the feasibility of applying the cylindrical magnetic drive mechanism in ESPs. Its non-contact transmission characteristic effectively solves dynamic seal leakage problems. The findings provide important insights for the design of magnetic drive systems in high-temperature downhole environments and hold significant value for engineering applications.

References

[1] W. S. Kim and J. E. Yun: CFD Analysis on the Balancing Hole Design for Magnetic Drive Centrifugal Pumps, Energies, Vol. 13 (2020) No.22, p.5865.

[2] X. H. Xu: Research and Application of a New Permanent Magnet Coupling, Inner Mongolia Coal Economy, (2019) No.6, p.22, 56.

[3] W. H. Yan, H. T. Yuan, J. Li et al.: Analysis of Torque Influencing Factors of Magnetic Drive Mechanism for Mud Power Generator, Journal of Xi'an Shiyou University (Natural Science Edition), Vol. 38 (2023) No.3, p.106-112.

[4] H. D. Wang: Energy Efficiency Optimization Design of Permanent Magnet Motor Drive System in Coal Mine Underground, China Coal Industry, (2025) No.08, p.68-69.

[5] Z. Fan: Discussion on the Application of Permanent Magnet Motor Drive in Belt Conveyors in Coal Mine Underground, Mechanical Management and Development, Vol. 38 (2023) No.4, p.230-231. DOI: 10.16525/j.cnki.cn14-1134/th.2023.04.096.

[6] Q. G. He, Q. K. Hong, Z. H. Zhou et al.: Comparative Analysis of Parameters of Plate Eddy Current Damping Units with Different Magnetic Circuit Structures, Journal of Hunan University (Natural Sciences), Vol. 52 (2025) No.11, p.101-117. DOI: 10.16339/j.cnki.hdxbzkb.2025109.

[7] H. Q. Wang, S. Y. Yu and G. Z. Zhou: Design of High-Efficiency Permanent Magnet Sealing Drive Magnetic Circuit Without Eddy Current, Journal of Magnetic Materials and Devices, Vol. 49 (2018) No.6, p.21-24. DOI: 10.19594/j.cnki.09.19701.2018.06.005.

[8] S. Z. Huang, B. Yu, J. D. Dong et al.: Rotor Topology Design and Strength Optimization Simulation of High-Speed Permanent Magnet Synchronous Motor, Explosion-Proof Electric Machine, Vol. 55 (2020) No.3, p.28-31.

[9] K. Z. Zhao: Magnetic Drive Technology and Equipment (Chemical Industry Press, China 2018).

[10] X. S. Dou, K. Z. Zhao and C. H. Xu: Magnetic Circuit Analysis and Magnetic Torque Calculation of Magnetic Drive Technology, Chemical Machinery, (2004) No.6, p.357-360.

[11] X. H. Ni, Y. T. Xu, B. Fu et al.: Magnetic Torque Characteristics Analysis and Configuration Optimization of Magnetic Drive Agitator, Process Equipment & Piping, Vol. 59 (2022) No.1, p.69-73, 80.